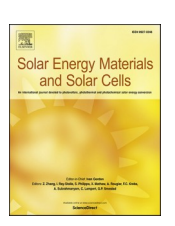
ELSEVIER

Contents lists available at ScienceDirect

### Solar Energy Materials and Solar Cells

journal homepage: http://www.elsevier.com/locate/solmat





# Room temperature synthesis of cesium lead bromide perovskite magic sized clusters with controlled ratio of carboxylic acid and benzylamine capping ligands

Ke Xu<sup>a,b</sup>, Evan T. Vickers<sup>b</sup>, Binbin Luo<sup>c</sup>, Qihui Wang<sup>a</sup>, A'Lester C. Allen<sup>b</sup>, Hongmei Wang<sup>d</sup>, Vivien Cherrette<sup>b</sup>, Xueming Li<sup>a,\*</sup>, Jin Zhong Zhang<sup>b,\*\*</sup>

- <sup>a</sup> College of Chemistry and Chemical Engineering, Chongqing University, Chongqing, 401331, PR China
- <sup>b</sup> Department of Chemistry and Biochemistry, University of California, Santa Cruz, CA, 95064, United States
- <sup>c</sup> Department of Chemistry, Shantou University, Guangdong, 515063, PR China
- <sup>d</sup> College of Biological, Chemical Sciences and Engineering, Jiaxing University, Jiaxing, 314001, PR China

#### ARTICLE INFO

#### Keywords:

Cesium lead bromide perovskite Perovskite magic sized clusters (PMSCs) Perovskite quantum dots (PQDs) Room temperature Controlled ratio of capping ligands

#### ABSTRACT

We demonstrate the synthesis of cesium lead bromide (CsPbBr<sub>3</sub>) perovskite magic sized clusters (PMSCs) and how to control the transformation from CsPbBr<sub>3</sub> perovskite quantum dots (PQDs) to PMSCs by varying the amount of organic carboxylic acids (CAs), including mesitylacetic acid (MAA), oleic acid (OA), and phenylacetic acid (PAA), along with benzylamine (BZA) as capping ligands at room temperature. The PQDs and PMSCs are characterized by means of XRD, UV/vis, photoluminescence (PL), time-resolved PL (TRPL), and X-rayphotoe-lectron spectroscopy (XPS). The concentration of CAs affects the excitonic absorption of both the CsPbBr<sub>3</sub> PMSCs ( $\lambda = 389-428$  nm) and CsPbBr<sub>3</sub> PQDs ( $\lambda = 460-516$  nm), with high concentration of CAs favoring CsPbBr<sub>3</sub> PMSCs over PQDs. With PAA at 45.45 mM, pure CsPbBr<sub>3</sub> PMSCs can be generated, which does not happen for MAA or OA, suggesting that PAA is a stronger ligand than MAA and OA. The results suggest that PMSCs require better passivation or stronger ligands than PQDs. This study establishes a simple and general method for synthesizing CsPbBr<sub>3</sub> PMSCs using a combination of BZA and CA capping ligands as a highly effective dual passivation system.

#### 1. Introduction

Magic sized clusters (MSCs), small nanoparticles with either single size or very narrow size distribution, serve as good model system for studying the transitions from atoms/molecules to larger structures such as quantum dots (QDs) or bulk material [1–5]. They can also be used as well-defined building blocks for fabricating large nanostructures for applications in fields such as photovoltaics, biosensors, light emitting diodes (LEDs) [1,6,7]. Today, MSCs of various II–VI compounds have been studied in terms of both chemical synthesis and theoretical investigations, such as CdSe, CdS, ZnS, ZnTe, and CdTe [6,8–14]. However, study of lead halide perovskite MSCs (PMSCs, APbX3; A = CH3NH3 and Cs; X = Cl, Br, and I) has been somewhat limted partly because their challenging synthesis [1,5,7,15]. Their structural characterization is also difficulty since they tend to grow into larger structures when dried

into solid form from solution [7]. Therefore, there is strong interest in developing an improved synthesis for perovskite QDs (PQDs) to PMSCs.

Recently, Yang's group proposed a synthesis method based on a high concentration of oleylamine (OLA) as capping ligand to obtain ultrasmall single-sized cesium lead bromide (CsPbBr<sub>3</sub>) PMSCs at room temperature [16]. Xu and co-workers reported the synthesis of  $\sim$ 2 nm CsPbBr<sub>3</sub> PMSCs using oleic acid (OA) and OLA capping ligands, and the PMSCs can be further converted to single-crystalline CsPbBr<sub>3</sub> quantum nanoribbons with bright deep-blue emission at room temperature [15]. Likewise, we have systhesized the methylammonium lead bromine (CH<sub>3</sub>NH<sub>3</sub>PbBr<sub>3</sub>) and CsPbBr<sub>3</sub> PMSCs and found a strong dependence on their capping ligand composition and concentration [1,7]. However, to our knowledge, there has been no study reported on the possible effect of using different capping ligands on synthesis of organo-metal halide PMSCs.

E-mail addresses: bbluo@stu.edu.cn (B. Luo), hongmei256@163.com (H. Wang), xuemingli@cqu.edu.cn (X. Li), zhang@ucsc.edu (J.Z. Zhang).

<sup>\*</sup> Corresponding author.

<sup>\*\*</sup> Corresponding author.

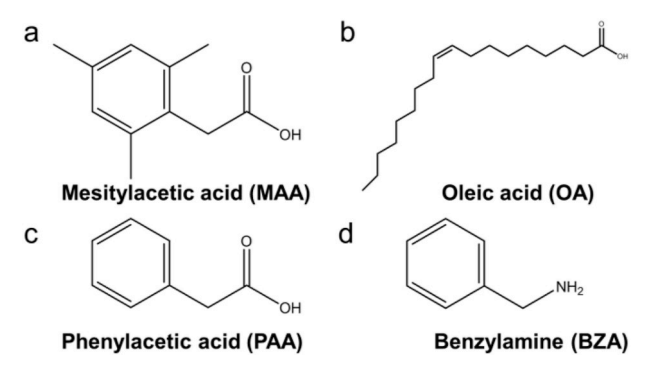


Fig. 1. Molecular structures of (a) mesitylacetic acid (MAA), (b) oleic acid (OA), (c) phenylacetic acid (PAA), and (d) benzylamine (BZA).

In this work, we demonstrate the synthesis of CsPbBr<sub>3</sub> PMSCs and their conversion to CsPbBr<sub>3</sub> PQDs by controlling the amount of organic carboxylic acids (CAs), including mesitylacetic acid (MAA), OA, and phenylacetic acid (PAA) together with benzylamine (BZA) as capping ligands at room temperature. The growth and optical properties of the PMSCs are found to be strongly dependent on the organic CAs used. High concentration of CAs favors CsPbBr<sub>3</sub> PMSCs over CsPbBr<sub>3</sub> PQDs. Pure

CsPbBr<sub>3</sub> PMSCs can be generated when the PAA concentration reaches 45.45 mM, which does not happen with OA or MAA, suggesting that PAA is a stronger ligand than MAA and OA. The results suggest that stronger binding ligands or higher concentration of ligands favors PMSCs over PODs, indicating PMSCs requires better passivation.

#### 2. Experimental methods

#### 2.1. Materials

Cesium bromide (CsBr, 99.9%, Strem Chemicals), lead bromide (PbBr<sub>2</sub>, 99.999%, Alfa Aesar), mesitylacetic acid (MAA, 98%,Alfa Aesar), oleic acid (OA, 98%, Fisher Chemical), phenylacetic acid (PAA, 99%, Aldrich), benzylamine (BZA, 99%, TCI), N,N-dimethylformamide (DMF, 99.5%, Fisher Scientific), toluene (100%, LabChem Inc). All the chemicals were used as received without further purification.

#### 2.2. Synthesis and purification of CsPbBr<sub>3</sub> PMSCs and CsPbBr<sub>3</sub> PQDs

CsPbBr $_3$  PMSCs and CsPbBr $_3$  PQDs were synthesized using a solvent reprecipitation method at room temperature condition [7,17]. CsBr (8.51 mg, 40  $\mu$ mol) and PbBr $_2$  (14.68 mg, 40  $\mu$ mol) were dissolved into 1.0 mL DMF to prepare the precursor solution. Next, 0.025 mmol PAA

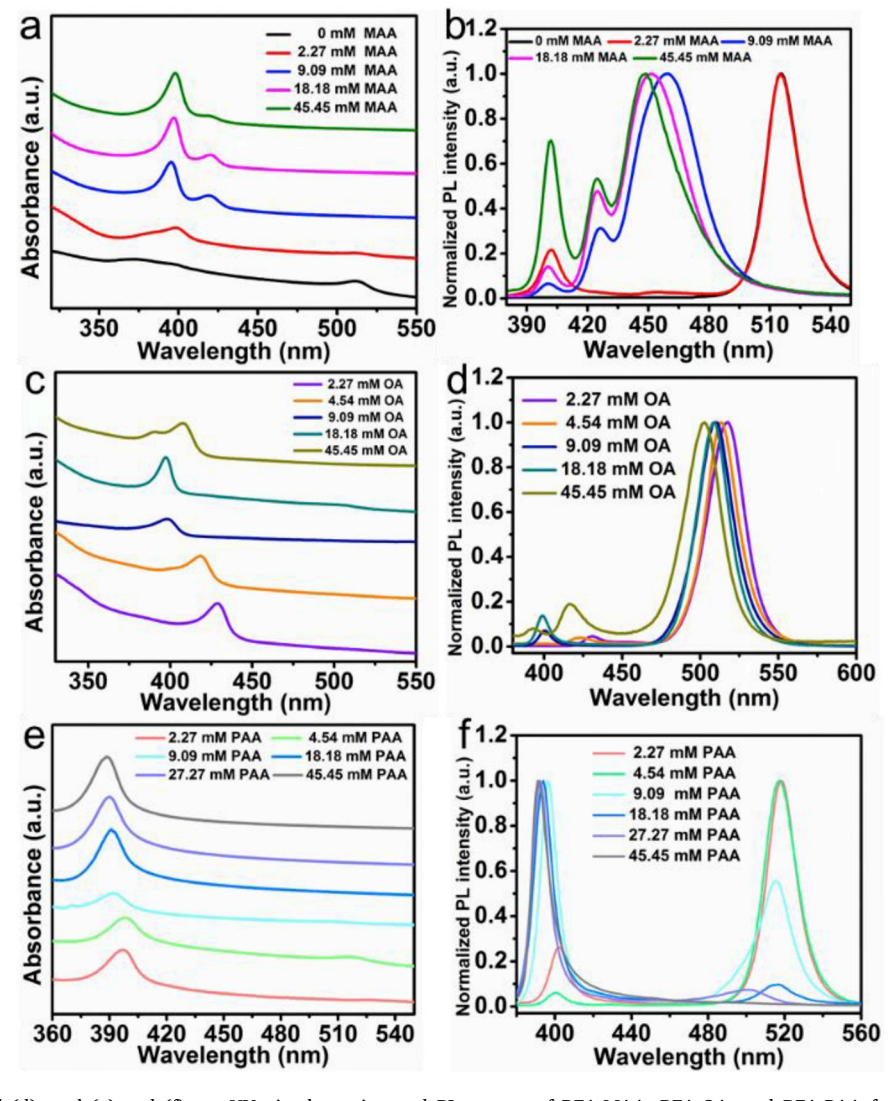


Fig. 2. (a) and (b), (c) and (d), and (e) and (f) are UV-vis absorption and PL spectra of BZA-MAA, BZA-OA, and BZA-PAA for CsPbBr<sub>3</sub> PQDs and CsPbBr<sub>3</sub> PMSCs samples.

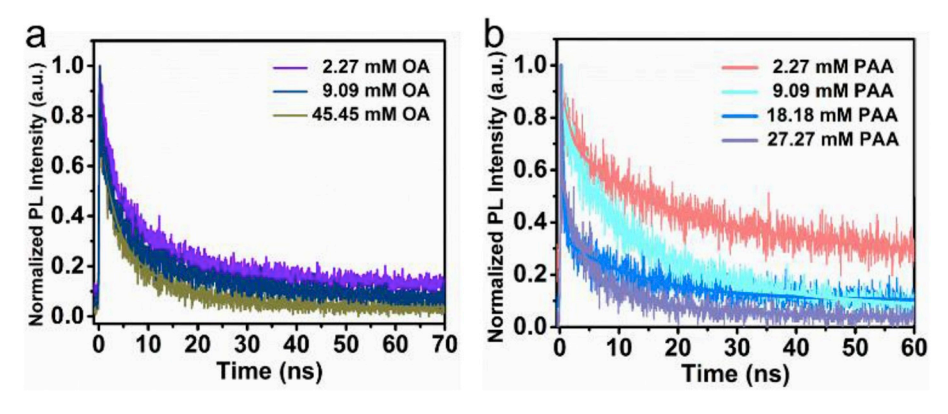


Fig. 3. Time-resolved photoluminescence decay curves of (a) BZA-OA and (b) BZA-PAA CsPbBr3 samples.

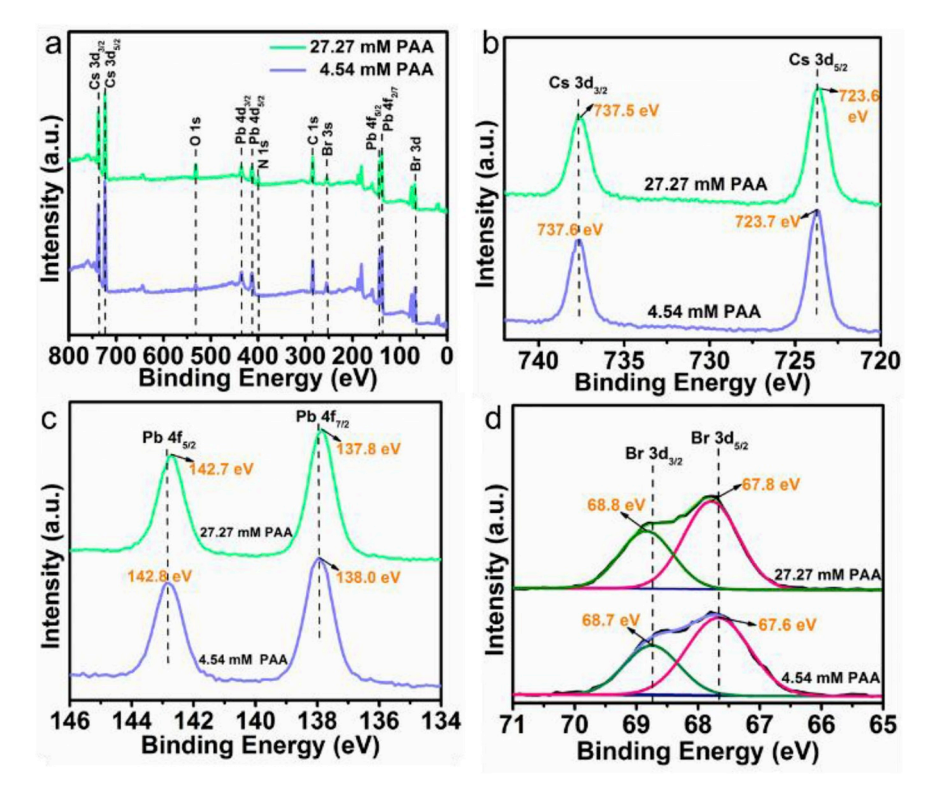


Fig. 4. (a) XPS survey spectra of BZA-PAA CsPbBr<sub>3</sub> PMSCs and PQDs. High resolution XPS analysis of BZA-PAA CsPbBr<sub>3</sub> PMSCs and PQDs corresponding to (b) Cs 3d, (c) Pb 4f, and (d) Br 3d.

and 0.001 mmol BZA were added to the precursor solution and dissolved. Then, the precursor solution was injected rapidly to 10.0 mL of toluene under vigorous stirring to obtain CsPbBr3 PMSCs and PQDs. Similarly, using the same amount of BZA, the amount of PAA was varied to 0.050, 0.100, 0.200, 0.300 and 0.500 mmol to synthesize BZA-PAA CsPbBr3 PMSCs and PQDs. For BZA-MAA and BZA-OA CsPbBr3 PMSCs and PODs. We also used the same amount 0.001 mmol BZA and changed the amount of MAA (0, 0.025, 0.100, 0.200, 0.500 mmol) and OA (0.025, 0.050, 0.100, 0.200, and 0.500 mmol) as capping ligands to add in CsBr (8.51 mg, 40  $\mu$ mol), PbBr<sub>2</sub> (14.68 mg, 40  $\mu$ mol) and 1.0 mL DMF to prepare the precursor solution, respectively. Then, the obtained BZA-MAA and BZA-OA precursor solution was injected rapidly to 10.0 mL of toluene under vigorous stirring to obtain CsPbBr3 PMSCs and PQDs. After completion of the reaction, the as-synthesized CsPbBr<sub>3</sub> PQDs and CsPbBr<sub>3</sub> PMSCs were centrifuged at a speed of 2000 rpm for 5 min in toluene. Finally, the supernatant was collected for the first wash, and after that, the precipitate was collected after each wash at a speed of 10000 rpm for 10 min in toluene to get perovskite powders and vacuum

drying at 25  $^{\circ}$ C for 8 h for further characterization. For the pure BZA-PAA CsPbBr<sub>3</sub> PMSCs sample, the particles are too small to be centrifuged, thus it is stored in the form of the liquid.

#### 2.3. Characterizations

Ultraviolet–visible (UV–vis) spectra were measured using UV–vis spectrometer (Agilent Technologies, Cary 60) and the fluorescence spectra were measured using a fluorometer (FluoroMax-3) using a quartz cuvette (1.0 cm  $\times$  1.0 cm) at room temperature. X-ray diffraction (XRD) data were acquired using a Rigaku American Miniflex Plus power diffractometer at a voltage of 40 kV and current of 30 mA, with scanning angle 10–60 (20) and rate of  $3^{\circ}$  min $^{-1}$ . X-ray photoelectron spectroscopy (XPS) measurements were performed by using a Thermo ESCALAB 250Xi spectrometer with an  $Al_{K\alpha}$  (1486.6 eV) excitation source to identify the chemical composition. Time correlated single photon counting (TCSPC) was measured by focusing on the sample using a 20  $\times$  objective with an effective power of 30 mW ( $\lambda_{ex}=500$  nm).

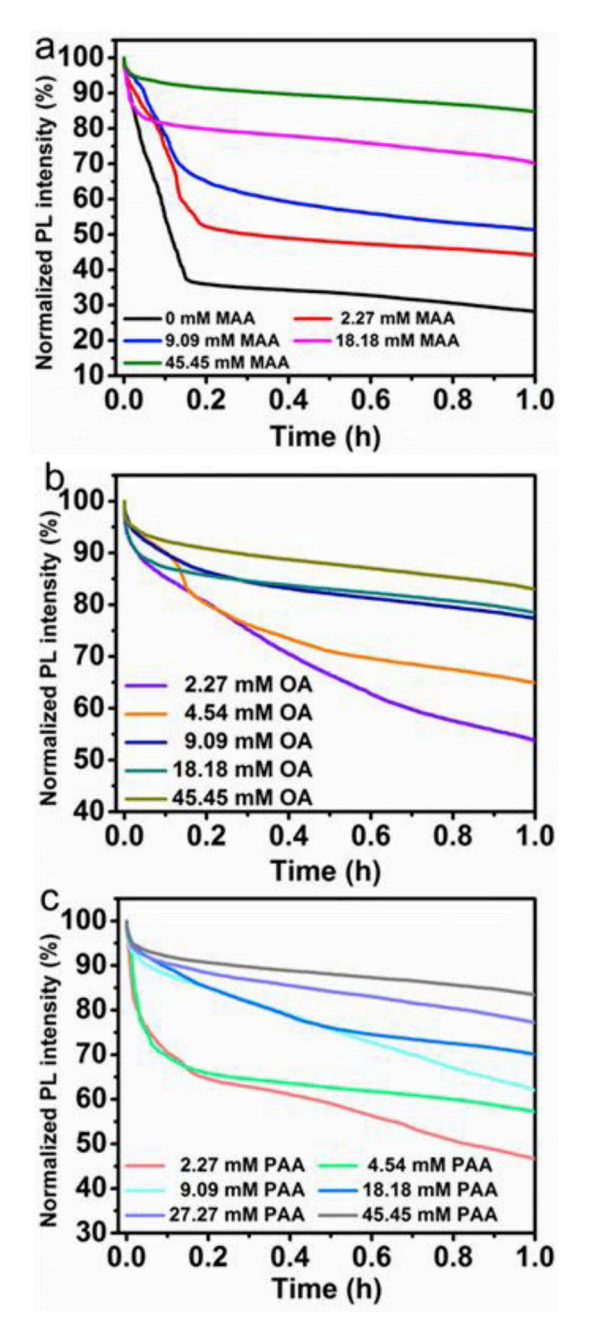


Fig. 5. Stability of BZA-MAA, BZA-OA, and BZA-PAA for  $CsPbBr_3$  PQDs and  $CsPbBr_3$  PMSCs solution in air and in the dark: the relative fluorescence intensity as a function of time.

#### 3. Results and discussion

## 3.1. Optical properties of $CsPbBr_3$ PQDs and PMSCs capped with CAs and BZA

The chemical molecular structures of the MAA, OA, PAA, and BZA ligands used in these experiments are shown in Fig. 1. To obtain PMSCs, excess amount of MAA/OA/PAA capping ligands together with BZA was used.

Fig. 2a and b shows the UV–vis absorption and photoluminescence (PL) spectra of BZA CsPbBr<sub>3</sub> PQDs as well as BZA-MAA CsPbBr<sub>3</sub> PQDs and PMSCs, respectively. In the UV–vis spectra of CsPbBr<sub>3</sub> PQDs with 0.091 mM BZA, there is a strong excitonic absorption peak at 512 nm. With the same amount BZA, increasing the amount of MAA from 2.27 to 9.09, 18.18, and 45.45 mM resulted in BZA-MAA CsPbBr<sub>3</sub> samples with

two or three excitonic absorption peaks, and the PL spectrum of each sample shows three emission peaks. For BZA-MAA CsPbBr<sub>3</sub> sample with a small amount of 2.27 mM MAA, there are three excitonic absorption peaks at 399, 460, and 511 nm, and the three PL emission peaks at 401, 461, and 514 nm. However, for with 9.09 mM MAA sample, there are two excitonic absorption peaks at 395 and 521 nm, and three PL emission peaks at 400, 425, and 459 nm. The very strong PL emission peak at 459 nm is not expected based on the two UV–vis peaks observed and may be due to trap states of CsPbBr<sub>3</sub> PMSCs or CsPbBr<sub>3</sub> PQDs formed from CsPbBr<sub>3</sub> PMSCs during the PL measurement. Details of the UV–vis and PL peaks of BZA-MAA CsPbBr<sub>3</sub> samples with different MAA concentrations are summarized in Table S1.

Fig. 2c and d shows the UV–vis absorption and PL spectra of BZA-OA CsPbBr $_3$  PQDs and PMSCs samples with different OA concentrations, and magnified PL emission peaks for BZA-OA CsPbBr $_3$  PMSCs sample in Fig. S1a. The detailed excitonic absorption peaks and PL emission peaks are summarized in Table S1. For the 18.18 mM OA sample, there are two excitonic absorption peaks at 397 and 505 nm, and two PL emission peaks at 398 and 509 nm. However, for other OA concentrations studied, there is an extra PL peak at around 510 nm, which could be due to trap states or PQDs formed during PL measurement.

Fig. 3a and b shows the UV–vis absorption and PL spectra of BZA-PAA CsPbBr $_3$  PQDs and PMSCs with different concentrations of PAA, and magnified PL emission peaks for BZA-PAA CsPbBr $_3$  PMSCs in Fig. S1b and detailed spectral features are summarized in Table S1. For the four samples with high PAA concentration, there is one excitonic absorption peak at around 395 nm, but two PL emission peaks at around 400 and 515 nm. The around 400 nm PL peak is attributed to excitonic emission while the around 515 nm peak could also be due to trap states or formed PQDs during PL measurement, similar to the BZA-MAA and BZA-OA CsPbBr $_3$  samples.

Based on previous studies, a 430–520 nm broader excitonic absorption peak is attributed to CsPbBr<sub>3</sub> PQDs, while the strong and sharp excitonic absorption peak at around 410 nm or bluer is assigned to CsPbBr<sub>3</sub> PMSCs [5,7,15,18–20]. Interestingly, with increasing amount of CAs for all BZA-MAA, BZA-OA and BZA-PAA samples, the PL emission peak shows a blue shift in the range of 430–518 nm. Compared with BZA-OA and BZA-PAA samples, BZA-MAA samples show a larger blue shift, indicative of smaller particles. The results also show that more CA capping ligands favor CsPbBr<sub>3</sub> PMSCs over CsPbBr<sub>3</sub> PQDs, as we found previously [7]. In addition, with an excess amount of MAA and OA, the synthesized product is a mixture of CsPbBr<sub>3</sub> PQDs and PMSCs. However, for 45.45 mM PAA, the synthesized product is pure CsPbBr<sub>3</sub> PMSCs, which suggests that different CAs affect the ratio between PQDs and PMSCs.

#### 3.2. Structural, dynamic, and electronic properties

Figures S2a, S2b and S2c compare the XRD patterns of BZA-MAA, BZA-OA and BZA-PAA CsPbBr<sub>3</sub> PQDs and PMSCs samples. The XRD pattern all show the main diffraction peaks at  $2\theta=15.2^{\circ}$ ,  $21.5^{\circ}$ ,  $26.3^{\circ}$ ,  $30.7^{\circ}$ ,  $37.6^{\circ}$  and  $43.7^{\circ}$ , corresponding to the interlayer spacing of the (100), (110), (111), (200), (211) and (202) crystal planes, respectively. These peaks comfirm the cubic phase structure with space group of Pm3 m (JCPDS No. 18–0364) [21,22]. However, all the samples also show some undetermined peaks, especially for the BZA-OA and BZA-PAA CsPbBr<sub>3</sub> samples. The undetermined peaks are most likely not from the original structures in solution but likely due to larger structures, such as aggregates, from CsPbBr<sub>3</sub> PMSCs upon drying to form the solid powders for XRD [7].

To better understand the dependence of the exciton lifetime on the amount of CAs, normalized time-resoved photoluminescence (TRPL) decay curves and related analysis data for BZA-OA and BZA-PAA CsPbBr<sub>3</sub> samples were carried out ( $\lambda_{ex}=500$  nm), as shown in Fig. 3 and Table S2. The PL decays were fitted using a double exponential function as given in Eq. (1) [2]:

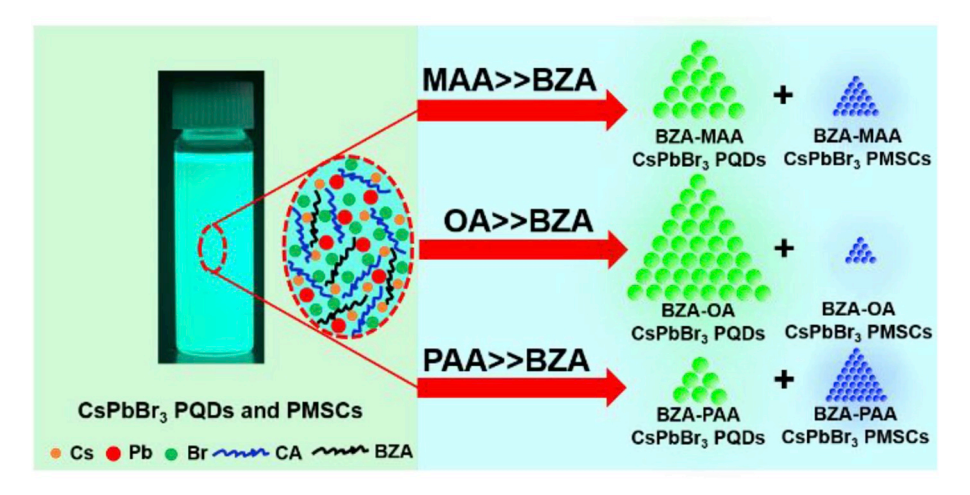


Fig. 6. Schematic illustration of the growth mechanism of CsPbBr<sub>3</sub> PQDs and CsPbBr<sub>3</sub> PMSCs at room temperature, and their dependence of transformation on the amount and type of CA.

$$I(t) = A_1 e^{(-t/\tau_1)} + A_2 e^{(-t/\tau_2)}$$
(1)

where  $A_1$  and  $A_2$  are the amplitudes of the fast and slow components (with  $A_1+A_2=1$ ); t is time; and  $\tau_1$  and  $\tau_2$  are the fast and slow decay lifetimes, respectively. All fitting parameters are reported in Table S2. The average lifetime ( $\tau_{ave}$ ) is calculated using Eq. (2) [23]:

$$\tau_{ave} = \frac{A_1 \tau_1^2 + A_2 \tau_2^2}{A_1 \tau_1 + A_2 \tau_2} \tag{2}$$

The  $\tau_{ave}$  for the BZA-OA and BZA-PAA CsPbBr $_3$  sample are calculated and shown in Table S2. With increasing CA concentration, the  $\tau_{ave}$  becomes shorter. The  $\tau_{ave}$  is determined by both radiative ( $\tau_{rr}$ ) and non-radiative ( $\tau_{rr}$ ) lifetime. According to previous reports,  $\tau_r$  is usually more dominated by the properties of the PQD core while  $\tau_{nr}$  is more sensitive to the type of capping ligands or surface properties and thereby surface passivation [2,23,24]. Specifically,  $\tau_r$  becomes longer with increasing PQD core size while  $\tau_{nr}$  becomes longer when there are less defects and better surface passivation [2,24]. For the BZA-OA and BZA-PAA samples, the excitonic emission peaks blue shift, indicating decreasing PQD size with increasing CA concentration, which should lead to shorter  $\tau_r$ . In the meantime, the BZA-OA and BZA-PAA samples have the same capping ligands, which should lead to similar  $\tau_{nr}$ . Therefore, variation in  $\tau_{ave}$  with CA concentration should be dominated by  $\tau_r$  or the PQD core size. According to following Eq. (3) [2]:

$$\frac{1}{\tau_{\text{cons}}} = \frac{1}{\tau_{\text{c}}} + \frac{1}{\tau_{\text{cr}}} \tag{3}$$

Therefore, it would expect  $\tau_{ave}$  to become shorter with increasing CA concentration, which is consistent with we have observed.

To further study the effectiveness of passivation of CAs and BZA, XPS survey spectra were obtained. As shown in Fig. 4a, for the BZA-PAA CsPbBr3 PMSCs and PQDs sample at 4.54 mM and 27.27 mM PAA, the main peaks of Cs 3d<sub>3/2</sub>, Cs 3d<sub>5/2</sub>, O 1s, Pb 4d<sub>3/2</sub>, Pb 4d<sub>5/2</sub>, N 1s, C 1s, Br 3s, Pb  $4f_{5/2}$ , Pb  $4f_{7/2}$  and Br 3d are observed, respectively [25–27]. For the low/high concentration of PAA samples, the binding energies of Cs  $3d_{5/2}$  and  $3d_{3/2}$  peaks in Fig. 4b appeared at 723.7/737.6 eV and 723.6/737.5 eV, respectively [27]. At the same time, for the low/high concentration of PAA smaples, the Pb  $4d_{7/2}$  and Pb  $4d_{5/2}$  peaks are observed at 138.0/142.8 eV and 137.8/142.7 eV in Fig. 4c, respectively, and the peaks at 67.6/68.7 eV and 67.8/68.8 eV corresponded to Br  $3d_{5/2}$  and Br  $3d_{3/2}$  binding energies in Fig. 4d [27]. Therefore, there are about 0.1/0.1 eV and 0.2/0.1 eV negative shifts for Cs 3d and Pb 4d for the low/high concentration of PAA samples, while there are about 0.2/0.1 eV positive shifts for Br 3d. This indicates that the electorn density around Cs 3d and Pb 4d increases while the electron density

around Br 3d decreases. This is consistent passivation of Cs<sup>+</sup> and Pb<sup>2+</sup> by -COO and Br by -NH<sub>3</sub> [2].

#### 3.3. Stability study

The environmental stability of metal halide perovskites is a major character of interest [2,28–31]. To evaluate their stability, the relative PL intensities of BZA-MAA, BZA-OA, and BZA-PAA CsPbBr<sub>3</sub> solutions were studied for 1.0 h in air and dark conditions, with the results shown in Fig. 5. For the BZA-MAA CsPbBr<sub>3</sub> samples with different amount of MAA as shown in Fig. 5a, the relative PL intensity decreased to about 28, 44, 51, 71 and 85% after 1.0 h, respectively. As shown in Fig. 5b, for the BZA-OA CsPbBr<sub>3</sub> samples with different amount of OA, the relative PL intensity of the solution decreased to 54, 65, 77, 79, and 83% after 1.0 h, respectively. Fig. 5c, shows the PL decay with time for the BZA-PAA CsPbBr<sub>3</sub> samples. The CsPbBr<sub>3</sub> can degrade in air under dark conditions due to possible reaction with oxygen [29]. The good stability of the pure BZA-PAA CsPbBr<sub>3</sub> MSCs and the mixture of CsPbBr<sub>3</sub> PMSCs and PQDs suggests that the CsPbBr<sub>3</sub> PMSCs stability in air is much better than that of CsPbBr<sub>3</sub> PQDs.

## 3.4. Dependence of surface passivation on CAs and ratio between CAs and BZA

Fig. 6 illustrates the typical procedure for synthesizing CsPbBr<sub>3</sub> PQDs and CsPbBr<sub>3</sub> PMSCs using BZA-MAA, BZA-OA and BZA-PAA as capping ligands. A higher concentration of CAs favors CsPbBr<sub>3</sub> PMSCs over PQDs, attributed to the fact that PMSCs have a larger surface-to-volume (S/V) ratio than PQDs [1,7]. In addition, PAA, together with BZA, can more eaily produce CsPbBr<sub>3</sub> PMSCs than MAA and OA due to its stronger acidity or binding ability of its conjugate base.

For effective passivation of PQDs or PMSCs, it is critical to use an acid and base pair [7]. In the current system, BZA is protonated with  $-NH_2$  becoming  $-NH_3^+$ , while CAs are deprotonated with -COOH becoming  $-COO^-$  [2]. The reactions can be described by Eq. (4):

$$C_6H_5CH_2NH_2 + R - COOH \rightarrow C_6H_5CH_2NH_3^+ + R - COO^-$$
 (4)

where R– means  $(CH_3)_3C_6H_5CH_2$ – for MAA,  $CH_3(CH_2)_7CH=CH(CH_2)_7$ – for OA, and  $C_6H_5CH_2$ – for PAA. RCOO<sup>-</sup> is expected to effectively passivate charged surface defects of  $Cs^+$  and  $Pb^{2+}$ , while  $C_6H_5CH_2NH_3^+$  for  $Br^-$ .

The dissociation constants for the acid  $(pK_a)$  and base  $(pK_b)$  are  $pK_a = 4.31$  for PAA, pKa = 5.02 for OA, and  $pK_b = 4.66$  for BZA [2,32,33]. Based on the molecular structure, we expect the acidity of MAA to be between PAA and OA, though the pKa of MAA cannot be found in

literature [34].Thus, the acidity of the three CAs is expected to be PAA > MAA > OA. Based on the calculation for the equilibrium constants ( $K_{eq}$ ) and the comparison of the  $K_{eq}$  values in SI 5, PAA deprotonates more eaily than OA or MAA when reacting with BZA, providing better passivation.

Furthermore, the ratio between CA and BZA is also found to be an important factor in the effectiveness of passivation. In most previous studies, the acid/base pair is based on OA/OLA with a ratio near 1 [17, 35,36]. In this study, the acid/case ratio is much higher than 1 for optimal passivation. This is possibly due to more  $\rm Cs^+$  and  $\rm Pb^{2+}$  surface defects and less  $\rm Br^-$  surface defects in the structure of  $\rm CsPbBr_3$  PMSCs. To understand better the exact structure of  $\rm CsPbBr_3$  PMSCs, further work will be needed in the future.

#### 4. Conclusion

In summary, we demonstarte the successful synthesis of CsPbBr<sub>3</sub> PMSCs and CsPbBr<sub>3</sub> PQDs using BZA-MAA, BZA-OA, and BZA-PAA as effective ligands at room temperature. The concentration of CAs affects the excitonic absorption of both CsPbBr<sub>3</sub> PMSCs and CsPbBr<sub>3</sub> PQDs, with high concentration of CAs favoring CsPbBr<sub>3</sub> PMSCs over PQDs, possibly due to PMSCs requiring better passivation than PQDs. Pure CsPbBr<sub>3</sub> PMSCs can be generated with 45.45 mM PAA, but not for MAA or OA at the same concentration, suggesting that PAA is a stronger ligand than MAA and OA, which likely passvates Cs<sup>+</sup> and Pb<sup>2+</sup> related surface defects. The results suggest that CsPbBr<sub>3</sub> PMSCs require better passivation (stronger or higher concentration of ligands) than CsPbBr<sub>3</sub> PQDs. This work demonstrates a simple and general method for synthesizing CsPbBr<sub>3</sub> PMSCs using a combination of BZA and CA capping ligands as a highly effective dual passivation system.

#### Declaration of competing interest

The authors declare that they have no known competing financial interests or personal relationships that could have appeared to influence the work reported in this paper.

#### Acknowledgements

This research was supported by NASA through MACES (NNX15AQ01A), NSF (CHE 1904547), the Fundamental Research Funds for the Central Universities (No.2018CDGFHG0012), JG2018103 (NO. SKL-ACPS-C-03) and a UCSC Committee on Research Special Research Grant. K.X. is grateful for financial support from the program of China Scholarship Council (CSC). B.L. thanks the support from the National Natural Science Foundation of China (NSFC: 51702205) and the STU Scientific Research Foundation for Talents (NTF17001). We thank Jeremy Barnett for help on the XRD test.

#### Appendix A. Supplementary data

Supplementary data to this article can be found online at https://doi.org/10.1016/j.solmat.2019.110341.

#### References

- E.T. Vickers, K. Xu, B.W. Dreskin, T.A. Graham, X. Li, J.Z. Zhang, Ligand dependent growth and optical properties of hybrid organo-metal halide perovskite magic sized clusters, J. Phys. Chem. C 123 (2019) 18746–18752.
- [2] K. Xu, E.T. Vickers, L. Rao, S.A. Lindley, A.C. Allen, B. Luo, X. Li, J.Z. Zhang, Synergistic surface passivation of CH<sub>3</sub>NH<sub>3</sub>PbBr<sub>3</sub> perovskite quantum dots with phosphonic acid and (3-aminopropyl)triethoxysilane, Chem. - Eur. J. 25 (2019) 5014–5021.
- [3] D.C. Gary, M.W. Terban, S.J.L. Billinge, B.M. Cossairt, Two-step nucleation and growth of InP quantum dots via magic-sized cluster intermediates, Chem. Mater. 27 (2015) 1432–1441.
- [4] D.R. Nevers, C.B. Williamson, B.H. Savitzky, I. Hadar, U. Banin, L.F. Kourkoutis, T. Hanrath, R.D. Robinson, Mesophase formation stabilizes high-purity magic-sized clusters, J. Am. Chem. Soc. 140 (2018) 3652–3662.

- [5] T.P. Nguyen, A. Ozturk, J. Park, W. Sohn, T.H. Lee, H.W. Jang, S.Y. Kim, Facile synthesis of CsPbBr<sub>3</sub>/PbSe composite clusters, Sci. Technol. Adv. Mater. 19 (2018) 10–17.
- [6] F. Muckel, J. Yang, S. Lorenz, W. Baek, H. Chang, T. Hyeon, G. Bacher, R. Fainblat, Digital doping in magic-sized CdSe clusters, ACS Nano 10 (2016) 7135–7141.
- [7] K. Xu, A.C. Allen, B. Luo, E.T. Vickers, Q. Wang, W.R. Hollingsworth, A.L. Ayzner, X. Li, J.Z. Zhang, Tuning from quantum dots to magic sized clusters of CsPbBr<sub>3</sub> using novel planar ligands based on trivalent nitrate coordination complex, J. Phys. Chem. Lett. 10 (2019) 4409–4416.
- [8] J. Eilers, E. Groeneveld, C. de Mello Donega, A. Meijerink, Optical properties of Mn-doped ZnTe magic size nanocrystals, J. Phys. Chem. Lett. 3 (2012) 1663–1667.
- [9] J.M. Azpiroz, J.M. Matxain, I. Infante, X. Lopez, J.M. Ugalde, A DFT/TDDFT study on the optoelectronic properties of the amine-capped magic (CdSe)<sub>13</sub> nanocluster, Phys. Chem. Chem. Phys. 15 (2013) 10996–11005.
- [10] S. Botti, M.A.L. Marques, Identification of fullerene-like CdSe nanoparticles from optical spectroscopy calculations, Phys. Rev. B 75 (2007).
- [11] M. Del Ben, R.W.A. Havenith, R. Broer, M. Stener, Density functional study on the morphology and photoabsorption of CdSe nanoclusters, J. Phys. Chem. C 115 (2011) 16782–16796.
- [12] E. Groeneveld, S. van Berkum, A. Meijerink, C. de Mello Donega, Growth and stability of ZnTe magic-size nanocrystals, Small 7 (2011) 1247–1256.
- [13] Y. Wang, Y.H. Liu, Y. Zhang, F. Wang, P.J. Kowalski, H.W. Rohrs, R.A. Loomis, M. L. Gross, W.E. Buhro, Isolation of the magic-size CdSe nanoclusters [(CdSe)<sub>13</sub>(n-octylamine)<sub>13</sub>] and [(CdSe)<sub>13</sub>(oleylamine)<sub>13</sub>], Angew Chem. Int. Ed. Engl. 51 (2012) 6154–6157.
- [14] C. Li, C. Han, Y. Zhang, Z. Zang, M. Wang, X. Tang, J. Du, Enhanced photoresponse of self-powered perovskite photodetector based on ZnO nanoparticles decorated CsPbBr<sub>3</sub> films, Sol. Energy Mater Sol. Cells 172 (2017) 341–346.
- [15] Y. Xu, Q. Zhang, L. Lv, W. Han, G. Wu, D. Yang, A. Dong, Synthesis of ultrasmall CsPbBr<sub>3</sub> nanoclusters and their transformation to highly deep-blue-emitting nanoribbons at room temperature, Nanoscale 9 (2017) 17248–17253.
- [16] L. Peng, J. Geng, L. Ai, Y. Zhang, R. Xie, W. Yang, Room temperature synthesis of ultra-small, near-unity single-sized lead halide perovskite quantum dots with wide color emission tunability, high color purity and high brightness, Nanotechnology 27 (2016) 335604.
- [17] X. Li, Y. Wu, S. Zhang, B. Cai, Y. Gu, J. Song, H. Zeng, CsPbX<sub>3</sub> quantum dots for lighting and displays: room-temperature synthesis, photoluminescence superiorities, underlying origins and white light-emitting diodes, Adv. Funct. Mater. 26 (2016) 2435–2445.
- [18] B. Luo, F. Li, K. Xu, Y. Guo, Y. Liu, Z. Xia, J.Z. Zhang, B-Site doped lead halide perovskites: synthesis, band engineering, photophysics, and light emission applications, J. Mater. Chem. C 7 (2019) 2781–2808.
- [19] L. Rao, Y. Tang, C. Yan, J. Li, G. Zhong, K. Tang, B. Yu, Z. Li, J.Z. Zhang, Tuning the emission spectrum of highly stable cesium lead halide perovskite nanocrystals through poly(lactic acid)-assisted anion-exchange reactions, J. Mater. Chem. C 6 (2018) 5375–5383.
- [20] H. Huang, H. Lin, S.V. Kershaw, A.S. Susha, W.C. Choy, A.L. Rogach, Polyhedral oligomeric silsesquioxane enhances the brightness of perovskite nanocrystal-based green light-emitting devices, J. Phys. Chem. Lett. 7 (2016) 4398–4404.
- [21] C.C. Stoumpos, C.D. Malliakas, J.A. Peters, Z. Liu, M. Sebastian, J. Im, T. C. Chasapis, A.C. Wibowo, D.Y. Chung, A.J. Freeman, B.W. Wessels, M. G. Kanatzidis, Crystal growth of the perovskite semiconductor CsPbBr<sub>3</sub>: a new material for high-energy radiation detection, Cryst. Growth Des. 13 (2013) 2722–2727.
- [22] J. Liu, L. Zhu, S. Xiang, Y. Wei, M. Xie, H. Liu, W. Li, H. Chen, Growing high-quality CsPbBr<sub>3</sub> by using porous CsPb<sub>2</sub>Br<sub>5</sub> as an intermediate: a promising light absorber in carbon-based perovskite solar cells, Sustain. Energy Fuels 3 (2019) 184–194.
- [23] H. Huang, A.S. Susha, S.V. Kershaw, T.F. Hung, A.L. Rogach, Control of emission color of high quantum yield CH<sub>3</sub>NH<sub>3</sub>PbBr<sub>3</sub> perovskite quantum dots by precipitation temperature, Adv. Sci. 2 (2015) 1500194.
- [24] S.B. Naghadeh, S. Sarang, A. Brewer, A. Allen, Y.H. Chiu, Y.J. Hsu, J.Y. Wu, S. Ghosh, J.Z. Zhang, Size and temperature dependence of photoluminescence of hybrid perovskite nanocrystals, J. Chem. Phys. 151 (2019) 154705.
- [25] M. He, Y. Cheng, R. Yuan, L. Zhou, J. Jiang, T. Xu, W. Chen, Z. Liu, W. Xiang, X. Liang, Mn-Doped cesium lead halide perovskite nanocrystals with dual-color emission for WLED, Dyes Pigm. 152 (2018) 146–154.
- [26] M. He, Y. Cheng, L. Shen, H. Zhang, C. Shen, W. Xiang, X. Liang, Doping manganese into CsPb(Cl/Br)<sub>3</sub> quantum dots glasses: dual-color emission and super thermal stability, J. Am. Ceram. Soc. 102 (2019) 1090–1100.
- [27] J. Liang, C. Wang, P. Zhao, Z. Lu, Y. Ma, Z. Xu, Y. Wang, H. Zhu, Y. Hu, G. Zhu, L. Ma, T. Chen, Z. Tie, J. Liu, Z. Jin, Solution synthesis and phase control of inorganic perovskites for high-performance optoelectronic devices, Nanoscale 9 (2017) 11841–11845.
- [28] Y. Chen, Y. Sun, J. Peng, W. Zhang, X. Su, K. Zheng, T. Pullerits, Z. Liang, Tailoring organic cation of 2D air-stable organometal halide perovskites for highly efficient planar solar cells, Adv. Energy Mater. 7 (2017) 1700162.
- [29] T. Leijtens, K. Bush, R. Cheacharoen, R. Beal, A. Bowring, M.D. McGehee, Towards enabling stable lead halide perovskite solar cells; interplay between structural, environmental, and thermal stability, J. Mater. Chem. 5 (2017) 11483–11500.
- [30] D. Wang, M. Wright, N.K. Elumalai, A. Uddin, Stability of perovskite solar cells, Sol. Energy Mater. Sol. Cells 147 (2016) 255–275.
- [31] N. Espinosa, L. Serrano-Luján, A. Urbina, F.C. Krebs, Solution and vapour deposited lead perovskite solar cells: ecotoxicity from a life cycle assessment perspective, Sol. Energy Mater. Sol. Cells 137 (2015) 303–310.

- [32] F.A. La Porta, R.T. Santiago, T.C. Ramalho, M.P. Freitas, E.F.F. Da Cunha, The role of the Frontier orbitals in acid-base chemistry of organic amines probed by ab initio and chemometric techniques, Int. J. Quantum Chem. 110 (2010), 2015-2023.
- [33] K.K. Athankar, K.L. Wasewar, M.N. Varma, D.Z. Shende, Separation of phenylacetic acid using tri-n-butyl phosphate in hexanol: equilibrium and kinetics, Sep. Sci. Technol. 52 (2017) 2696–2703.
- [34] X. Chen, D. Xing, L. Zhang, R.I. Cukier, Y. Bu, Effect of metal ions on radical type and proton-coupled electron transfer channel: sigma-radical vs pi-radical and
- sigma-channel vs pi-channel in the imide units, J. Comput. Chem. 30 (2009) 2694–2705
- [35] L. Rao, X. Ding, X. Du, G. Liang, Y. Tang, K. Tang, J.Z. Zhang, Ultrasonication-assisted synthesis of CsPbBr<sub>3</sub> and Cs<sub>4</sub>PbBr<sub>6</sub> perovskite nanocrystals and their reversible transformation, Beilstein J. Nanotechnol. 10 (2019) 666–676.
- [36] J.S. Yao, J. Ge, B.N. Han, K.H. Wang, H.B. Yao, H.L. Yu, J.H. Li, B.S. Zhu, J.Z. Song, C. Chen, Q. Zhang, H.B. Zeng, Y. Luo, S.H. Yu, Ce<sup>3+</sup>-Doping to modulate photoluminescence kinetics for efficient CsPbBr<sub>3</sub> nanocrystals based light-emitting diodes, J. Am. Chem. Soc. 140 (2018) 3626–3634.